Optik - International Journal for Light and Electron Optics 224 (2020) 165426

Contents lists available at ScienceDirect

Optik

journal homepage: www.elsevier.com/locate/ijleo

Original research article

Facile Synthesis of ZnO/AC Nanocomposites using *Prosopis Juliflora* for Enhanced Photocatalytic Degradation of Methylene Blue and Antibacterial Activity

S. Sheik Mydeen [a], R. Raj Kumar [b], S. Sambathkumar [c], M. Kottaisamy [d], V. S. Vasantha [e,*]

[a] *Department of Chemistry, Sethu Institute of Technology, Pulloor, Kariapatti, 626 115, Tamil Nadu, India*
[b] *Institute of Medical Engineering, Department of Biophysics, School of Basic Medical Sciences, Health Science Center, Xi'an Jiaotong University, Xi'an, 710061, Shaanxi, PR China*
[c] *Department of Chemistry, Vivekanandha College of Arts and Sciences for Women (Autonomous), Tiruchengode, Namakkal 637 205, Tamil Nadu, India*
[d] *Department of Chemistry, Thiagarajar College of Engineering, Madurai 625 015, Tamil Nadu, India*
[e] *School of Chemistry, Madurai Kamaraj University, Palkalainagar, Madurai 625 021, Tamil Nadu, India*

ARTICLE INFO

Keywords:
ZnO
Carbon nanocomposite
Surface oxygen vacancy
Photocatalysis
Antibacterial activity

ABSTRACT

A facile synthesis of ZnO/activated carbon (ZnO/AC) nanocomposites has been made using the stem of *Prosopis Juliflora* by one-pot synthetic method. These composite materials have been characterized by various techniques such as X-ray diffraction (XRD), Fourier transform- infrared spectroscopy (FT-IR), Scanning electron microscopy (SEM), Diffuse reflectance spectroscopy (DRS) and Photoluminescence (PL) respectively. The morphology of ZnO nanocrystal exhibits flower like architecture with controlled size and shape. The photocatalytic performance of ZnO/AC has been analyzed with different proportions (1%, 3%, 5%) on methylene blue (MB) dye under ultraviolet radiation. The photocatalytic activity is greatly influenced by band gap, crystal size and surface oxygen vacancies (SOv) of the nanocomposites. The rate of photodegradation is 92.2 % at 45 min for 3% carbon in ZnO/AC material and it is 10% higher than that of pristine ZnO. Moreover, the photo degradation of MB has been investigated with various pH like 2.5, 3.5, 7, 8.5, 9.5 and the adsorption efficiency of ZnO based on surface zero point charge in acidic and basic medium has been discussed. Additionally, the antibacterial activity of the ZnO/AC nanocomposites has been carried out against *Pseudomonas aeruginosa* and the result shows improved antibacterial activity with the increase in carbon percentage.

1. Introduction

The wastewater from various industries contains toxic organic pollutants which cause severe environmental pollution [1,2]. The organic dyes present in the effluents are hard to degrade, due to their chemical stabilities. Many processes, including adsorption [3], chemical oxidation [4], ion-exchange [5], reverse osmosis [6], precipitation [7], biological [8] and photocatalytic treatments have been developed to treat the organic dye contaminated in water [9]. Among the methods proposed so far, semiconductor based

* Corresponding author.
E-mail address: vasantham999@yahoo.co.in (V.S. Vasantha).

https://doi.org/10.1016/j.ijleo.2020.165426
Received 20 June 2020; Received in revised form 11 August 2020; Accepted 12 August 2020
Available online 18 August 2020

photocatalysis for the degradation of organic dyes has received considerable attention, due its high efficiency and low cost [10–13]. Although TiO_2 has been widely investigated, zinc oxide (ZnO) has received significant attraction as an efficient catalyst for the photo degradation of organic contaminants present in water because it is relatively inexpensive. Further, nano-sized ZnO exhibits wide band gap, high specific surface area and high surface activity and the photocatalytic mechanism is similar to that of TiO_2 [14,15]. Furthermore, many reports have been highlighted that ZnO exhibits higher efficiency than TiO_2 in the photocatalytic degradation of organic dyes present in the wastewater [16]. However, in reality, one essential problem to be settled to further improve how their performance is to retard the recombination of the photogenerated electrons and holes [17]. Many efforts have been reported to prevent the quick recombination of electron-hole pairs, such as using semiconductor hybrids with noble metals, metal oxide and carbon materials and found that the concentration of carbon materials in the starting solution also plays an important role in photoelectronic and photocatalytic performance of the composites. The property of semiconductor surface depends on the effective adsorption of organic pollutants, otherwise hinders the dispersion into the catalyst and may affect the photocatalytic process. Activated carbon (AC) behaves as the support for ZnO, which results over the other medium. Because, AC has high surface area, porosity and also adsorbs pollutants rapidly. In nanocomposites, AC helps to enhance the adsorption of pollutant and metal oxide to degrade the pollutants and product discharging from the surface [18–21].

P. juliflora plants are developed in a wide range of soil conditions, including waste lands and they withstand in yearly temperature ranges from 14 to 34 °C with the rainfall of 50 to 1,200 mm [22]. Moreover, ZnO has considered as a promising material for anti-bacterial, anticancer and food packaging [23]. Owing to its biosafety, biocompatibility and bioactivity against microorganisms, ZnO has received considerable attention to antibacterial studies under ultraviolet, visible and absence of light [24]. The ZnO nanoparticles have surface oxygen defects and large surface area and they possesses efficient contact with microbes than microparticles [25]. Many reports have been proposed on the antibacterial mechanism of ZnO and found oxidative stress due to reactive oxygen species (ROS) [26,27]; dissolution of Zinc ion [28] efficiently behaves in bacteria to ruptures the bacterial cells [29,30]. Herein, we made facile one-pot synthesis of ZnO/AC nanocomposites using the stem of *Prosopis Juliflora* and characterized. Consequently, the crystal size, surface morphology, band gap and surface oxygen vacancies are examined systematically. The photocatalytic degradation of MB and antibacterial activity has been presented.

2. Experimental Section

2.1. Materials

Zinc acetate (Zn $(CH_3COO)_2$. $2H_2O$) (99%), sodium hydroxide (98.5%), Cetrimide (99%), Con .H_2SO_4 (98%), and other chemicals have also been purchased with analytical grade from Merck and used without further purifications.

2.2. Preparation of Activated Carbon

Fresh stem of *Prosopis juliflora* plant was washed, dried and powdered using mortar, and subsequently soaked in a 50% of sulfuric acid. Then, resulting powder was washed with double distilled (DD) water to remove the acidity until the filtrate turns neutral and heated at 750 °C in a tubular furnace under N_2 atmosphere. The gas flow rate was set to 150 °C/min for an hour and was allowed to cool down in the air at an ambient temperature to obtain plant-derived activated carbon (PAC).

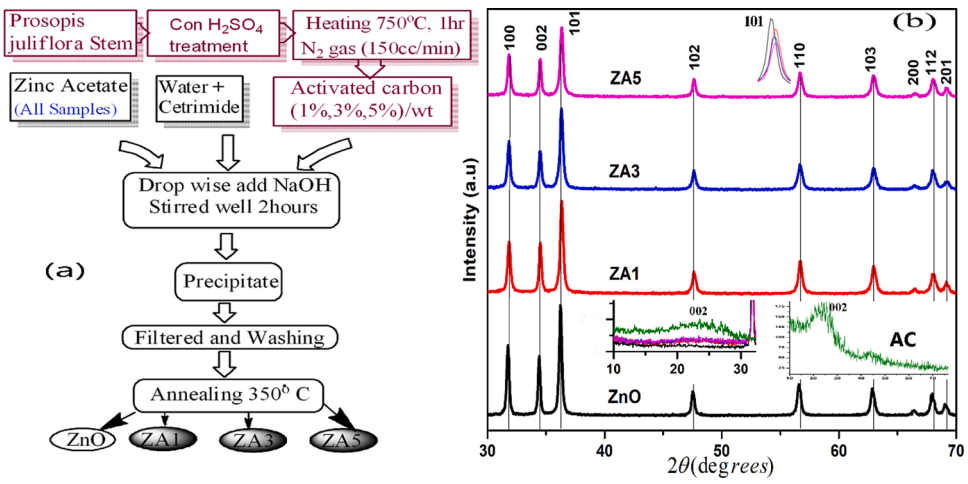

Fig. 1. (a) Schematic representation of ZnO/AC synthesis; (b) XRD pattern of AC, ZnO and ZnO/AC nanocomposites.

2.3. Preparation of ZnO/AC Nanocomposites

For the preparation of ZnO photocatalyst, the solution of Zinc acetate (0.07 M) in DD water was mixed with 0.01 M cetrimide and stirred for 2 hours. Then, it was added with activated carbon with different proportions 1%, 3%, 5%. Then, 0.15 M of NaOH in distilled water was slowly added to the precursor. The resulting precipitate was filtered and washed thoroughly with DD water and dried by heating with 60 °C for few hours. Finally, the sample was annealed at the 350 °C in a muffle furnace for 2 hours and labeled as ZA1. The same procedure was followed for ZA3, ZA5 are shown in Fig. 1(a). For comparison, pure ZnO was also prepared without the addition of activated carbon.

2.4. Characterization Techniques

X-ray studies were performed using a PAN analytical X'Pert PRO with Cu Kα radiation (λ=1.5418 Å) using 20 mA, with an accelerating voltage of 40 kV at a scanning rate of 2°/min. The chemical nature of the sample was analyzed by SHIMADZU 8400 FT-IR Spectrometric Analyzer using the KBr pellet method. Morphology of the samples was analyzed using a JEOL JSM-6380 LV scanning electron microscope, which was operated at an accelerating voltage of 20 kV. UV–Visible diffuse reflectance spectra were recorded on a Shimadzu UV-2450 Spectrophotometer equipped with an integrating sphere. The Photoluminescence was recorded at room temperature by utilizing Varian Cary Eclipse Spectrophotometer.

2.5. Photocatalytic Performances

The Photocatalytic degradation was carried out using a homemade photo catalytic reactor of a 100 mL cylindrical flask and a pen type UV lamp (365 nm) was immersed in the middle of the flask. 0.25 g/L of the catalyst was added to methylene blue solution (2×10^{-5} M), and pH of the solution was measured to be 6. To ensure the adsorption equilibrium, the solution was stirred for about 30 min. prior to irradiation. The solution was subjected to UV illumination and air was purged to maintain the homogeneous suspension and absorption spectra of the samples were taken for every 15 min..

2.6. Antibacterial Activity

The antibacterial activity has been performed on *Pseudomonas aeruginosa* bacteria by disc diffusion technique. The Mueller Hinton broth (LB) dilution scheme was used to find minimal inhibitory concentrations (MIC) and it was verified. Further, volatile fractions were confirmed [31]. All test approaches were achieved like LB supplemented with Tween 80 (5%) [32]. The bacterial strains were cultured in the lab at overnight in LB at 37 °C. Tubes of the LB method with various concentrations of extract solution were inoculated with 10 mL of 10^{-5} CFU/mL using standard microorganisms suspensions. This bacterial culture was used specially incubated with a shaker (120 RPM) at 37 °C for 24 hours [33]. The Control tubes also examined with absence of samples simultaneously. The experiments were repeated as triplicate for the same procedure. The MIC was characterized as the most minimal concentration growth prevention [34]. According to the reports, the tubes showing with complete absence of growth were identified and incubated.

3. Results and discussion

3.1. XRD Characterization

The XRD pattern obtained for the AC, ZnO and ZnO/AC are shown in Fig. 1(b). Clearly, the XRD patterns of the tested samples matched well with pure ZnO (JCPDS 36-1451). The peaks observed in 2θ values (1 0 1) plane confirmed the formation of hexagonal wurtzite type structure of ZnO of all the samples. The 2θ values detected for ZnO/AC nanocomposites were originated to be the same plane for the pure ZnO. Thus, the incorporation of activated carbon did not alter the crystalline of zinc oxide. The broad peak was around 26 (corresponds to the activated carbon plane of (0 0 2) [35]. No impurity peaks were observed, thereby indicating that the final material was a combination for ZnO and ZnO/AC with high purity. When compared the 1 0 1 planes of all samples, the carbon percentage depends on the decrease in peak height. These may be the reason to change the crystallinity and high defects in ZnO/AC nanocomposites compared to ZA3, exhibits low crystal size but high dislocation density. They are listed in Table 1.

Table 1
Structural parameters of the pure and ZnO/AC nanocomposites.

Samples	Crystallite size $D = 0.9\lambda/\beta\cos\theta$ (nm)	Dislocation density $\delta = 1/D^2$ (X 10^{14}Lines/m^2)	Reference
ZnO	56.9	3.3748	[36]
ZA1	60	2.8802	
ZA3	52.8	3.8715	
ZA5	59.3	2.9272	

3.2. FT-IR Spectroscopic Analysis

Fourier transform-infrared spectroscopy has been used to identify the organic and inorganic functional materials present in the samples. Fig. 2. depicts the FT-IR spectra of the pure ZnO and different percentages ZnO/AC from the wavenumber ranges 400-4000 cm^{-1}. ZA3 sample has a broad absorption peak around 3446 cm^{-1} and this stretching of OH groups may be adsorbed water molecule. All samples have CO_2 group observed in the peaks at 2363 cm^{-1} except for ZA3 and such peak resulting the decomposition of the acetate group. The peak observed in 1591 cm^{-1} corresponds to the C = C stretching and supports the percentage of carbon increase in the composites. The lower frequency region peaks at 902 and 445 cm^{-1} corresponds to Zn–C and Zn–O respectively [37–39].

3.3. Photoluminescence Spectroscopic Analysis

Photoluminescence spectra of ZnO/AC and ZnO nanoparticles are shown in Fig. 3a. In general, the peak observed in the UV region is usually attributed to the band edge transition or exciton recombination. Peaks in the visible emission are termed as deep level emission and usually attributed to intrinsic and extrinsic defects in ZnO. It can be seen that ZnO/AC and ZnO samples exhibit peaks at 393, 438, 490 and 520 nm [40]. The ZnO has a solid absorption band at 325 nm, which records the excitation wavelength of the PL spectra at room temperature and UV emission peak centered at 393 nm is attributed to exciton recombination. The emission band at 438 nm is attributed to the violet emission originated from transitions involving zinc interstitial defects or oxygen interstitials. The next lower energy absorption bands such as blue 490 nm and green 520 nm emission bands are most likely due to the presence of SOv [41].

3.4. DRS Analysis

Diffuse reflectance spectra of the ZnO/AC and ZnO are shown in Fig. 3b. The absorption peaks are shifted towards longer wavelength from 384 to 390 nm, when the concentration of activated carbon has increased from 1% to 3%. The optical band gap is evaluated using the tauc plot [42]. Fig. 3c. represents the values which are found to be 3.24, 3.23 and 3.25 eV for 1%, 3%, 5% of activated carbon and 3.26 eV for ZnO. The band gap decreases, when the carbon content increases from 1% to 3%, which enhance the photocatalytic performance, because carbon suppresses the recombination of electron-hole pairs upon absorption. The ZnO/AC samples peak exhibits red shift towards longer wavelength with the increase of carbon percentage and also compared with pristine ZnO. The absorption edge of the ZA5 samples blue shifted to shorter wavelength due to lowest oxygen vacancy. J Wang *et.al* reported the oxygen vacancies ranges from higher wavelength absorption of ZnO, and the band gap appears to be narrow, which is closely related to the oxygen vacancy. i.e., ZA3 has the highest oxygen vacancy concentration response to the best higher wavelength light response [43].

3.5. Morphological Characteristics

Morphological features of the ZnO/AC have been investigated by SEM analysis shown in Fig. 4. The Pure ZnO is agglomerated and the particle length is 1200 nm, diameter is 100 nm. The ZnO/AC composite i.e. ZA1, ZA3, ZA5 lengths are 727, 1125 and 545 nm, but the diameter found to be 68, 46 and 56 nm respectively. It can be seen that the bare ZnO nanoparticles display flower petals shaped morphology and it is obviously demonstrated that the particles are aggregated. However, the introduction of carbon has decreases the aggregation which could be observed from the SEM image [35]. As the carbon percentage increases from 1% to 5%, the flower petals

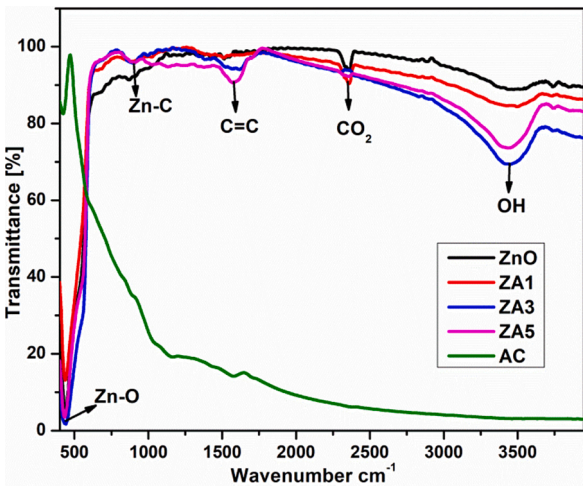

Fig. 2. FT-IR spectra of AC, ZnO and ZnO/AC nanocomposites.

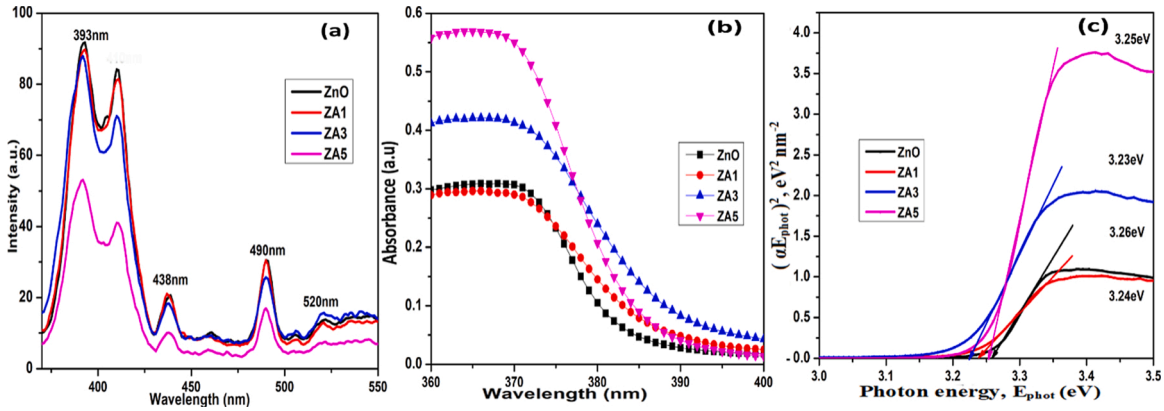

Fig. 3. (a) PL spectra; (b) DRS spectra; (c) direct band gap of the ZnO/AC and ZnO.

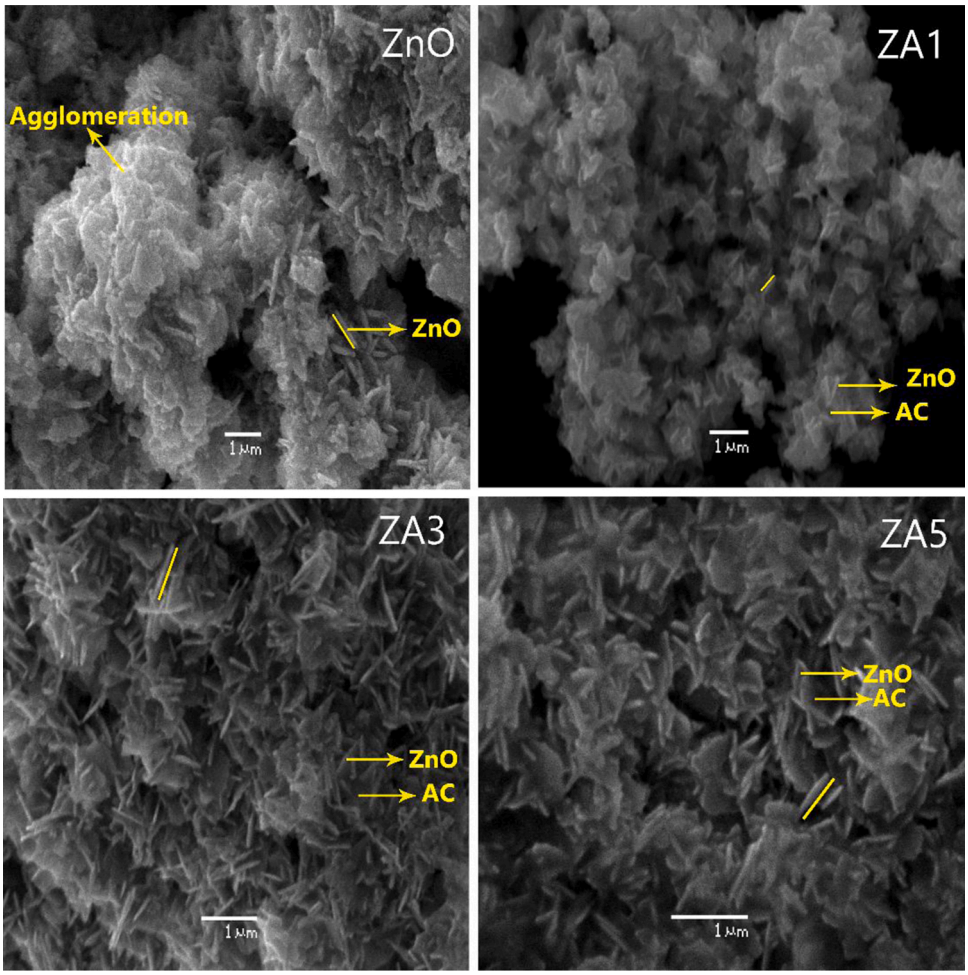

Fig. 4. SEM images obtained for ZnO and ZnO/AC nanocomposites.

are separated from one another. Thus, higher percentage of carbon in nanocomposites observed, due to the surface area of individual flower shaped petals has increased and it is has been observed in the SEM image.

3.5.1. EDX Analysis

In order to understand the chemical composition of ZnO and ZnO/AC nanocomposite, the EDX and elemental analysis were

determined, and the results are tabulated in Fig. 5. The elements present in the ZnO/AC nanocomposite are Zn, O and C and ZnO has Zn and O as the constituents. From this result, it is clearly found that the atomic composition of ZA3 has maximum oxygen vacancies when compared to other samples. The ZA5 sample has a lower oxygen vacancy among ZnO/AC nanocomposites and ZnO have least oxygen vacancies among the investigated samples.

3.6. Photodegradation of methylene blue

The Photocatalytic activity of the pristine ZnO and ZnO/AC nanocomposites on methylene blue has been studied under dark and UV illumination. Fig. 7e. shows that in dark condition, MB removal percentage has increases with the activated carbon 1%, 3% and 5%. It reveals that the percentage of carbon increases with the adsorption of MB on the surface of ZnO/AC nanocomposites. The photocatalytic activity has been carried out in 45 min. under UV light irradiation and the MB concentration has been maintained at 2×10^{-5} M for all the samples. The removal rate is decreased with the following order ZA3 > ZA1 > ZA5 > ZnO. The higher percentage of activated carbon samples has high adsorption of MB and more active sites for the chemical degradation and they are related to earlier studies. Then, the rates of MB removal continuously expanding ZA3 with preferred 92.2% over other nanocomposites. This result supports that ZA3 nanocomposite has optimum band gap as well as the surface defect sites and oxygen vacancy shown in EDX spectra. The photoluminescence spectra favors the ZA5 sample to inhibit the excited electron. However, ZA5 sample has a high percentage of AC to reduce the photocatalytic activity due to UV light introduction on ZnO is diminished and also lower oxygen vacancy compared to ZA1 and ZA3.

To investigate the photocatalytic mechanism of ZnO/AC nanocomposites, trapping experiments has been carried out. As shown in Fig. 6, triethanolamine (TA) performed as a hole scavenger (h^+), benzoquinone (BQ) as the superoxide ion radical ($O_2\cdot$) and *t*-butyl alcohol (TBA) as the hydroxyl radical (OH·) scavenger. While addition of TA and TBA in the solution, the photocatalytic efficiency has decreased slightly for ZnO/AC nanocomposites, which reveals that, BQ is responsible for significant decrease in photocatalytic performance. Thus, $O_2\cdot$ plays a vital role in the photocatalytic mechanism in ZnO/AC nanocomposites. Moreover, $O_2\cdot$ found to be dominant in ZA3 among the ZnO/AC nanocomposites. This result correlated with highest oxygen vacancy in ZA3, evident from EDX spectra. But, h^+ behaves as a dominant role in pristine ZnO. It is clearly understood that the activated carbon with the help of oxygen vacancy easily adsorb excited electron from the valence band to the conduction band and inhibit the recombination of electrons.

Fig. 7f represents MB adsorbed by the surface of ZnO/AC nanocomposites under UV light illumination. The PL and EDX spectra show the SOv in nanocomposites, which supports for rising maximum valence band. Hence, band gap energy distance has decreased. For this reason, Valence band to the conduction band charge separation is very easy and efficiency of photo hole pair (h^+) is also increased [14] as in Equation (1). This hole pair (h^+) decomposes the water molecule to form OH radical as shown in Equation (2). The PL spectra indicates that the inhibition of recombination ability increases with the increasing carbon percentage, this result shows the excited electron trap has completed by the activated carbon and also oxygen sites of formation of superoxide ($O_2^{\cdot -}$) as shown in Equation. (3), (4) and (5) [44]. Therefore, the recombination of excited electron has reduced. Finally, OH and O_2^- radicals are decomposed by the surface adsorbed MB dye [45] as shown in Equation (6) and (7).

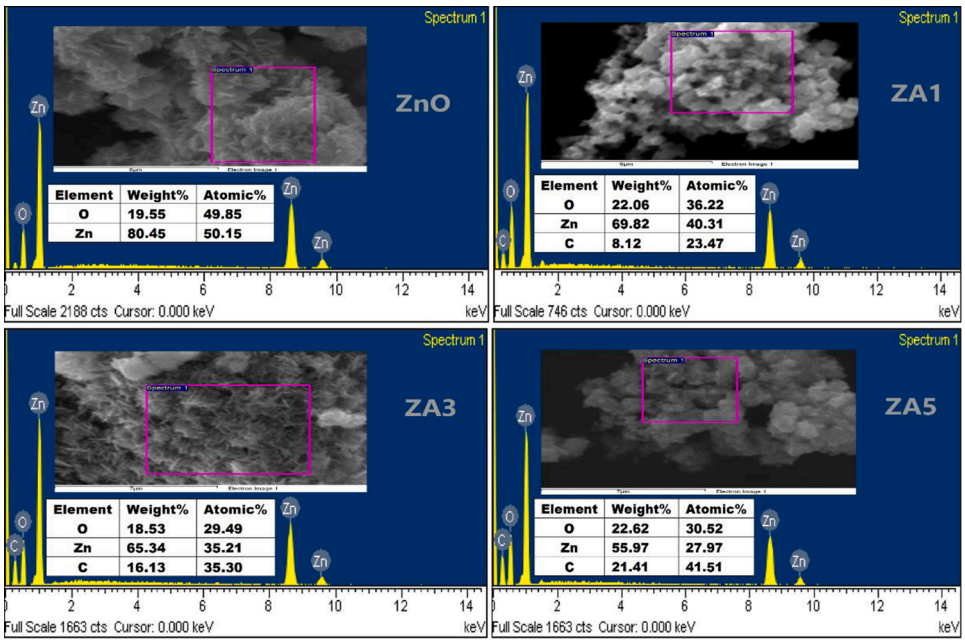

Fig. 5. EDX spectra of ZnO and ZnO/AC nanocomposites.

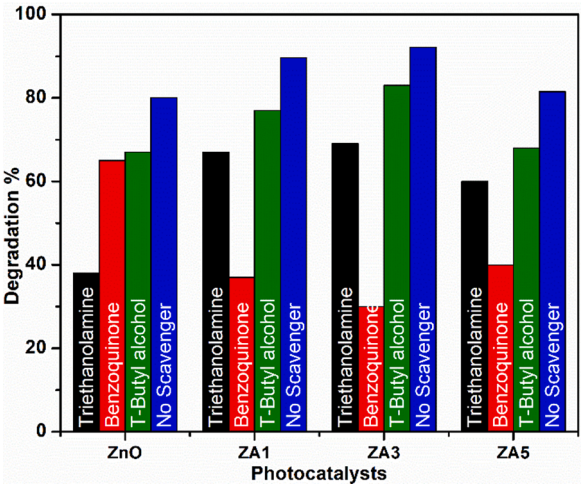

Fig. 6. Effects of scavengers on photocatalytic degradation efficiency of MB by using ZnO, ZA1, ZA3 and ZA5 under UV light irradiation; (MB: 2×10^{-5}M, contact time: 45 min and catalyst: 250 mg/L, pH-6).

$$ZnO(VB) + h\nu \rightarrow ZnO(h^{+}VB) + ZnO(e^{-}\ CB) \quad (1)$$

$$ZnO(h^{+}VB) + H_2O \rightarrow OH^{\cdot} \quad (2)$$

$$ZnO(e^{-}CB) \rightarrow AC^{\cdot} \quad (3)$$

$$ZnO(e^{-}\ CB) + O_2 \rightarrow O_2^{\cdot -} \quad (4)$$

$$AC^{\cdot} + O_2 \rightarrow O_2^{\cdot -} \quad (5)$$

$$O_2^{\cdot -} + MB \rightarrow CO_2 + H_2O \quad (6)$$

$$OH + MB \rightarrow CO_2 + H_2O \quad (7)$$

Fig. 8 illustrates MB dye removal percentage which has been increased with the increase of pH value in an acidic medium and the presence of ZnO/AC shows better photocatalytic activity. A.F Alkaim *et al.* have reported that ZnO adsorption capacity in the MB dye molecule increases the pH from 2 to 9.5 [46]. The surface of ZnO adsorption behavior depends on the point zero charge (pzc) value of ZnO and it is 8.3 [47]. The surface of ZnO charge compared to pH solution at pH < pHpzc, has positive charge. Similarly, at pH > pHpzc the catalyst surface has negatively charged. For the pH value below 8.3, at acidic condition, the ZnO surface has a positive charge and attracts only negative dye molecule. Unfortunately, the MB dye molecule has a cationic charge and decreases the electrostatic attraction between dye and pristine ZnO catalyst. But, ZA3 sample has activated carbon and it helps the adsorption of dye molecule. Hence, better photo degradation occurs than pristine ZnO [48]. At pH 8.3, the pristine ZnO surface has a negative charge to improve photocatalytic activity in basic medium, because, the cationic MB adsorption increases. Moreover, the basic medium contains OH^{-} ion which involves in photocatalytic mechanism and it increases the photocatalytic activity. Thus, in acidic medium activated carbon only helps to enhance the adsorption of MB for the ZnO/AC, exhibits better photocatalytic activity in acidic medium compared to pristine ZnO [13].

3.7. Reusability of the Catalyst

The reusability of photocatalyst has received significant attention towards economic aspects so, photocatalyst efficiency has been analyzed. For this purpose, the cycling stability of ZA3 nanocomposite and pristine ZnO has been evaluated for four cycles under irradiation of UV light with 45 min for each cycle. Upon comparison of both samples, the degradation rate of MB is tested. After four cycles, the stability of ZnO in acidic medium is very poor and possesses low degradation compared to ZA3 nanocomposite. Hence, the removal rate of ZA3 after the fourth cycle has reached 70%, but pristine ZnO has attained 10% only, which has been shown in Fig. 9. This result reveals that the ZA3 nanocomposite has better reusability in acidic medium compared to pristine ZnO.

Some reported metal oxide nanocomposites for photocatalytic degradation of dyes are tabulated (Table 2) and found that the degradation rate of the catalyst results depends on catalyst loading, pH, dye concentration, time and light sources used.

3.8. Antibacterial activity

Antibacterial studies were carried out against *Pseudomonas aeruginosa* due to its better reaction towards nano-ZnO, in our previous work reported by using disc diffusion method [52]. As shown in Fig. 10 and Table 3, the antimicrobial activities of ZnO and nanocomposites are tested against *P. aeruginosa* with tetracycline as standard. The concentration ranges from 1 mg to 1 pg mg/mL has been

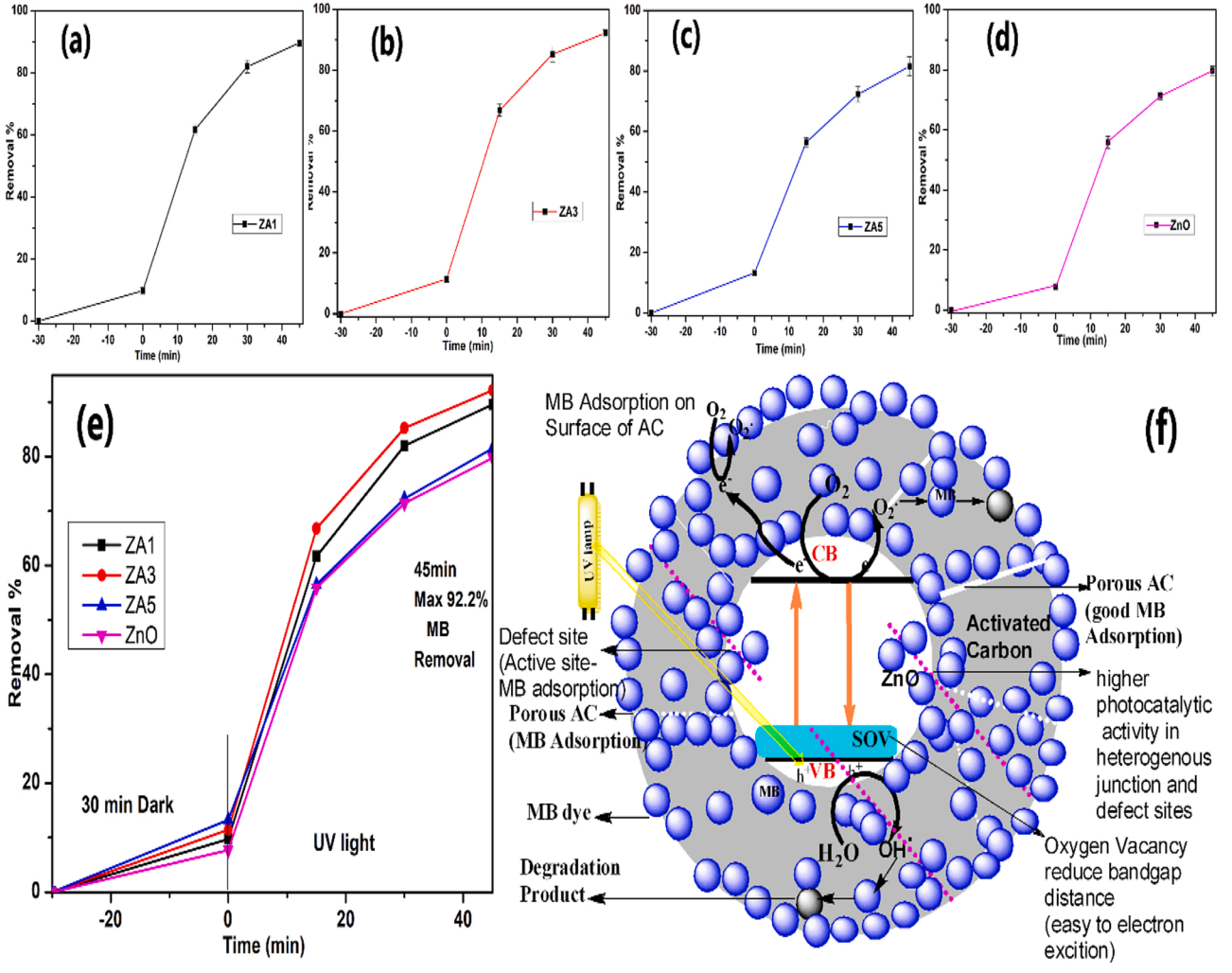

Fig. 7. (a, b, c, d) Photodegradation of MB dye error bars of ZA1,ZA3, ZA5 and ZnO; (e) Effect of dose of MB concentration 2×10^{-5}M, contact time: 45 min and dose of the catalyst: 250 mg/L, pH-6; (f) Representation of ZnO/AC photocatalytic processes.

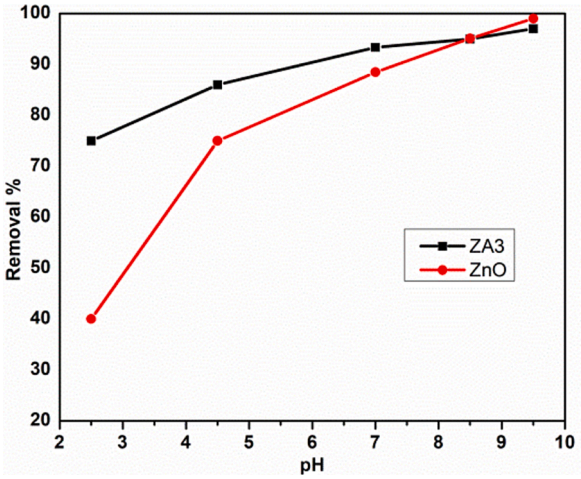

Fig. 8. Effect of dose of MB concentration 2×10^{-5} M, contact time: 45 min and dose of the catalyst: 250 mg/L.

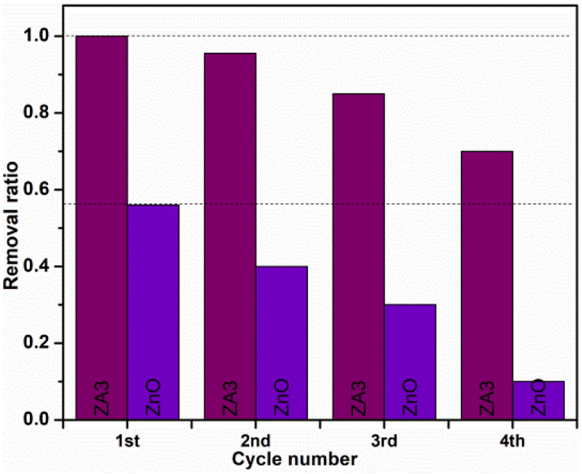

Fig. 9. Stability investigation of MB by ZA3 composite and pristine ZnO at pH 3.

Table 2
Studies with some metal oxide nanocomposites against degradation of dye.

Catalyst	Dye Concentration	Light source	Degradation rate and time	Reference
ZnO/CuO = 0.1 g/200 mL water	RhB, 1×10^{-5}mol·L	UV light (Hg lamp, 100 W, 365 nm)	60% achieved in 140 min.	[49]
ZnO/CuO = 0.1 g/300 mL water	RhB, 1×10^{-5}mol·L	Sun light 750 lux.	97.8% achieved in 100 min.	
SnO(12.7 wt%)/ZnO = 150 mg/300 mL water	2 mL RhB solution (4.89 ppm)	Sun light 950 lux	100% achieved in 60 min.	[50]
ZnO/M1(MXene) = 35 mg/50mL	RhB, 10 mg/L	Visible light (xenon lamp, 300 W, 420 nm)	98% achieved in 80 min.	[51]
ZnO/AC = 25 mg/100 mLwater	MB, 2×10^{-5} M	UV light (Hg lamp, 30 W, 365 nm)	92.2%,achieved in 45 min.	Present work

analyzed. The synthesized nanocomposites shows effective antimicrobial activity against the standard microorganisms compared to tetracycline itself. The measurements of zone of inhibition (nm) are recorded in Table 3 as the mean and standard deviation.

The obtained result shows that the increasing carbon percentage of nanocomposites are directly proportional to antibacterial activity. The result of trapping method formation of super oxide radical of reactive oxygen species (ROS) O_2^{-} also form in dark condition [53]. It reveals that the ZnO/AC samples with high production of ROS radicals, due to the high percentage of Carbon, which reflects to destroy the bacteria. This result is similar to the results reported by Lakshmi Prasanna et al. and which means that the

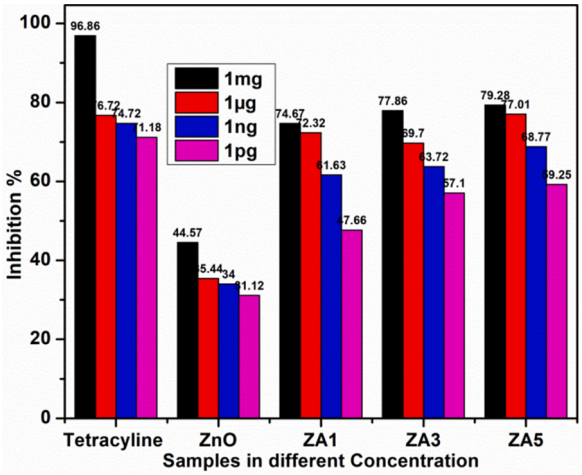

Fig. 10. Antibacterial activity of the ZnO and ZnO/AC nanocomposites.

Table 3
Antibacterial activity of *P. aeruginosa* for minimum inhibition concentration (MIC) with different concentrations of ZnO and ZnO/AC.

Tested Bacteria	Tested Samples	Zone of inhibition			
		1mg/mL	1µg/mL	1ng/mL	1pg/mL
P. aeruginosa	Tetracyline antibiotics	96.86	76.72	74.72	71.18
	ZnO	44.47	41.46	36.44	34.45
	ZA1	74.67	69.7	61.63	47.66
	ZA3	77.86	72.12	63.72	57.10
	ZA5	79.28	77.01	68.77	59.25

production of ROS radical is formed by the involvement of superoxide radical in the presence of surface of oxygen defects of ZnO in dark condition [54]. The creation of oxygen demand is higher in the bacteria respiration chain and finally, the bacterial cell damaged.

Generally, the gram negative bacteria of the *Pseudomonas aeruginosa's* outer wall contains lipoteichoic acid and it has a rich negative cell wall as well as it contain poly anions. These anions may possibly be attaching ZnO nanoparticles. Furthermore, this acid dissolution of ZnO happens to form of Zn^{2+} ions. After that, this transport of metal ion from the outer membrane reaches the inner membrane through the bacterial transport mechanism. This transfer of Zn^{2+} binds with ATP and increases the concentration of Zn^{2+} with toxicity effect as well as killing the bacteria [55]. The ZnO/AC nanocomposite sample production of Zn^{2+} and ROS with two ways is to attack *Pseudomonas aeruginosa* bacteria. Since, the ZnO/AC sample has better antibacterial activity than ZnO.

4. Conclusion

A new flower-petal type ZnO/AC nanocomposites have been prepared using *Prosopis Juliflora* stem *via* coprecipitation method. The chemical structure of the obtained nanocomposites has been thoroughly investigated with different analytical and spectroscopic techniques. The photo reactivity of the ZnO/AC nanocomposites has been studied *via* the photodegradation of MB under UV radiation. The ZA3 nanocomposite is found to be better degradation ability owing to oxygen vacancy was observed from EDX and DRS spectra. The AC enhances the MB adsorption and the oxygen vacancies in ZnO/AC has assisted to boost the optical achievement of photocatalyst in an acidic medium and basic medium has zero point charge achieved good photocatalytic in pristine ZnO. Thus, ZA3 nanocomposite has 92.2% degradation which reaches at 45 mins and it has compared to 10% higher than Pristine ZnO in pH 6 and also low pH. The ZnO/AC nanocomposites exhibits higher antimicrobial activity against *Pseudomonas aeruginosa* bacteria, since the percentage of carbon increases in the under dark condition. ZnO/AC has turned the band gap and the surface oxygen defects based formation of radicals of Zn^{2+}, ZnO-ROS involves a better antibacterial mechanism. Therefore, lower concentration catalyst enhances the better antibacterial activity than pristine ZnO. Thus, the ZnO/AC nanocomposites have possible applications in photocatalysis for wastewater treatment, and antimicrobial activity for therapeutic and diagnostic applications.

Declaration of Competing Interest

The authors report no declarations of interest.

References

[1] J. Tian, Y.H. Sang, G.W. Yu, H.D. Jiang, X.N. Mu, H. Liu, Adv. Mater. 25 (2013) 5074–5083.
[2] A. Mohammad, K. Kapoor, S.M. Mobin, Chem. Select 1 (2016) 3483–3490.
[3] M.T. Yagub, T.K. Sen, S.A, H.M. Ang, Adv. Colloids Interface Sci. 209 (2014) 172–184.
[4] R. Vedachalam, S. Karuppiah, Der PharmaChemica 9 (1) (2017) 53–58.
[5] M.A. Khan, M.I. Khan, S. Zafar, Memb. Water Treat. 8 (3) (2017) 259–277.
[6] M.F. Abid, M.A. Zablouk, A.M. Abid-Alamee, Irani. J. of Envir. Health Sci. &Engi. 9 (17) (2012).
[7] M.X. Zhu, Li Lee, H.H. Wang, Z. Wang, J. of Haza. Mat. 19 (2007) 735–741.
[8] D. Bhatia, N.R. Sharma, J. Singh, R.S. Kanwar, J. Crit, Rev. in Environ. Sci. and Tech. 47 (19) (2017) 1836–1876.
[9] S. Prabhu, S. Megala, S. Harish, M. Navaneethan, P. Maadeswaran, S. Sohila, R. Ramesh, Appl. Surf. Sci. 487 (2019) 1279–1288.
[10] C. Eley, T. Li, F. Liao, S.M. Fairclough, J.M. Smith, G. Smith, S.C.E. Tsang, Angew. Chem. Int. Ed. 53 (2014) 7838–7842.
[11] K. Zheng, H. Liu, C. Nie, X. Zhang, H. Hu, G. Ma, H. Wang, J. Huo, Mater. Lett. 253 (2019) 30.
[12] Y. Wang, R. Shi, J. Lin, Y. Zhu, Energy Environ. Sci. 4 (2011) 2922–2929.
[13] R. Cai, B. Zhang, J. Shi, M. Li, Z. He, ACS Sustainable Chem. Eng. 5 (2017) 7690–7699.
[14] H. Wang, G.B. Yi, X.H. Zu, X.M. Jiang, Z. Zhang, H.S. Luo, Mater. Lett. 138 (2015) 204–207.
[15] N. Daneshvar, D. Salari, A.R. Khataee, J. Photochem. Photobiol. A. 162 (2004) 317–322.
[16] S. Lam, J. Sina, A.Z. Abdullah, A.R. Mohamed, Desali. And Water Treat. 41 (1–3) (2012) 131–169.
[17] K. Karthik, S. Dhanuskodi, S. Prabukumar, S. Sivaramakrishnan, Optik 204 (2020) 164221.
[18] A. Nayak, B. Bhushan, V. Gupta, P. Sharma, J. Colloid Interface Sci. 493 (2017) 228–240.
[19] J.G. McEvoy, W. Cui, Z. Zhang, Appl.Cat. B: Envir. 144 (2014) 702–712.
[20] D.H. Quinones, A. Rey, P.M. Alvarez, F.J. Beltran, P.K. Plucinski, App. Cata. B: Envir. 144 (2014) 96–106.
[21] L. Zhang, L. Du, X. Yu, S. Tan, X. Cai, P. Yang, Y. Gu, W. Mai, ACS Appl. Mater. Interfaces. 6 (2014) 3623–3629.
[22] N.M. Pasiecznik, P. Felker, G. Harsh, L.N. Harris, J.C. Cruz, K. Tewari, A Monograph, HIDRA. In The Prosopis Juliflora-Prosopis Pallida Complex, United Kingdom, Coventry, 2001.
[23] M. Miyauchi, A. Nakajima, T. Watanabe, K. Hashimoto, Chem. Mater. 14 (2002) 2812–2816.
[24] K.R. Raghupathi, R.T. Koodali, A.C. Manna, Langmuir 27 (2011) 4020–4028.
[25] N. Padmavathy, R. Vijayaraghavan, Sci. Technol. Adv. Mater. 9 (3) (2008), 035004.
[26] G. Applerot, A. Lipovsky, R. Dror, N. Perkas, Y. Nitzan, R. Lubart, A. Gedank, Adv. Funct. Mater. 19 (2009) 842–852.
[27] M. Li, L. Zhu, D. Lin, Environ. Sci. Technol. 45 (2011) 1977–1983.
[28] R. Brayner, R. Ferrari-Iliou, N. Brivois, S. Djediat, M.F. Benedetti, F. Fievet, Nano. Lett. 6 (2006) 866–870.
[29] L.K. Adams, D.Y. Lyon, P.J.J. Alvarez, Water. Res. 40 (2006) 3527–3532.
[30] Y. Li, J. Niu, W. Zhang, L. Zhang, E. Shang, Langmuir 30 (2014) 2852–2862.
[31] S. Burt, Int. J. Food Microbiol. 94 (3) (2004) 223–253.
[32] F. Hicheri, H. Ben Jannet, J. Cheriaa, S. Jegham, Z. Mighri, C R Chimi. 6 (2003) 473–483.
[33] J. May, C.H. Chan, A. King, L. Williams, G.L. French, J. Antimicro. Chem. 45 (5) (2000) 639–643.
[34] P.J. Delaquis, K. Stanich, B. Girard, G. Mazza, Int. J. Food Microbiol. 74 (1-2) (2002) 101–109.
[35] B. Xing, C. Shi, C. Zhang, G. Yi, L. Chen, H. Guo, G. Huang, J. CaO, J. Nanomater. (2016) 1–10.
[36] K. Karthik, P. Maria, P. Nikolova, A. Phuruangrat, S. Pushpa, V. Revathi, M. Subbulakshmi, Mater. Res. Innov. (2019) 1–6.
[37] M. Vinayagam, S. Ramachandran, V. Ramya, A. Sivasamy, J. Environ. Chem. Eng. 6 (3) (2018) 3726–3734.
[38] K. Intarasuwan, P. Amornpitoksuk, S. Suwanboon, P. Graidist, S. Maungchanburi, C. Randorn, Adv. Pow. Tech. 29 (11) (2018) 2583–2904.
[39] S.H. Largani, M.A. Pasha, Int. Nano. Lett. 7 (2017) 25–33.
[40] B.L. Atul, S.M. Yuvaraj, J. Saud. Chemi. Soc. 19 (2015) 471–478.
[41] S. Kumar, N. Reddy, H. Kushwaha, A. Kumar, M. Shankar, K. Bhattacharyya, A. Halder, V. Krishnan, Chem. Sus. Chem. 10 (2017) 3588–3603.
[42] R.R. Kanna, N. Lenin, V. Sakthipandi, M. Sivabharathy, Ceram. Int. 43 (2017) 15868–15879.
[43] J. Wang, Z. Wang, B. Huang, Y. Ma, Y. Liu, X. Qin, X. Zhang, Y. Dai, ACS Appl. Mater. Interfaces 4 (2012) 4024–4030.
[44] P. Li, F. Liu, Y. Liu, R. Xue, X. Fan, J. of Dispersion Sci. and Tech. (2020), https://doi.org/10.1080/01932691.2019.1711110.
[45] Q. Zhang, M. Xu, B. You, Q. Zhang, H. Yuan, K. Ken Ostrikov, Appl. Sci. 8 (2018) 353.
[46] A.F. Alkaim, A.M. Aljeboree, N.A. Alrazaq, S.J. Baqir, F.H. Hussein, A.J. Lilo, Asian J. Chem. 26 (24) (2014) 8445–8448.
[47] M. Farrokhi, S.C. Hosseini, J.K. Yang, M. Shirzad-Siboni, Water, Air, & Soil Pollution 225 (9) (2014).
[48] D.K. Lee, S.C. Kim, S.J. Kim, I.S. Chung, S.W. Kim, Chem. Eng. J. 102 (1) (2004) 93–98.
[49] C. Chen, X. Liu, Q. Fang, X. Chen, T. Liu, M. Zhang, Vacuum 174 (2020) 109198.
[50] C. Chen, W. Mei, C. Wang, Z. Yang, X. Chen, X. Chen, T. Liu, J. Alloys compd. 826 (2020), 154122.
[51] X. Liu, C. Chen, Mater.Lett. 261 (2020), 127127.
[52] S.S. Mydeen, M. Kottaisamy, V.S. Vasantha, Intern J Innov Tech and Expl Eng. 9 (2) (2019) 930–938.
[53] J. Gupta, D. Bahadur, ACS Omega 3 (2018) 2956–2965.
[54] V.L. Prasanna, R. Vijayaraghavan, Langmuir 31 (2015) 9155–9162.
[55] V. Revathi, K. Karthik, Chemical Data Collections. 21 (2019) 100229.